Spontaneous motion of a droplet evolved by resonant oscillation of a vortex pair

Takahiko Ban,[1,*] Yosuke Hatada,[1] and Katsuroku Takahashi[2]
[1]*Department of Chemical Engineering & Materials Science, Doshisha University 1-3 Tatara Miyakodani, Kyotanabe, Kyoto, 610-0321 Japan*
[2]*Department of Human Environment Design, Sugiyama Jogakuen University, Hoshigaoka Motomachi 17-3, Chikusa, Nagoya, 464-8662 Japan*

(Received 5 September 2008; revised manuscript received 8 December 2008; published 4 March 2009)

We studied dissipative structures in the pattern formation of self-organized flow inside a droplet and spontaneous motion of the droplet when two driving forces, mass transfer of a solute from the droplet to surrounding media and continuous supply of solution to the droplet, were applied. When solute concentration increases beyond a critical value, a jetlike flow erupts out of the droplet (eruption). A similar flow simultaneously enters the droplet (irruption), producing internal flow. The resulting internal flow develops into two vortices along the droplet surface. Each vortex moves in a circular orbit along the droplet surface by local flow due to the other vortex, while continuous solute eruptions occur out of the vortex pair. The entire droplet rotates slowly at the same velocity as the rotation of the vortex pair. The vortex pair then oscillates with rotation, inducing droplet wiggle with slow rotation. The vortex motion resembles precession accompanied by nutation of a spinning top about a fixed point. Temporal evolution of droplet motion describes a pattern of short waves superimposed on a long wave. Short waves are induced by "nutation" of the vortex pair, and the long wave by "precession." The amplitude of the short wave varies with time because of the interaction between vortices. The vortex pair acts as coupled oscillators. Resonance interaction can occur between the long wave and the envelope of short waves when the phase velocity of the long wave becomes equal to the group velocity of short waves, markedly changing droplet motion; vigorous and regular fast rotation of the droplet suddenly occurs.

DOI: 10.1103/PhysRevE.79.031602 PACS number(s): 68.05.−n, 05.65.+b, 83.60.Wc, 05.70.Ln

I. INTRODUCTION

Spontaneous fluid flow induced by interfacial instability is a well-known phenomenon occurring under chemical and physical nonequilibrium conditions [1–7]. Although the flow develops locally, it can enhance mass transfer rate or induce a net mass transport of liquids. When a droplet is formed in the immiscible liquid phase, interfacial motion is observed as spontaneous motion of the entire droplet. Droplet motions are erratic and intermittent, known as the "kicking" phenomenon. Lewis and Pratt first observed that a pendant droplet containing solute, which diffuses into the surrounding continuous phase, sometimes showed ripples and pulsations [7]. They suggested that the effect of the heat produced in transfer caused local variations in interfacial tension, thereby disturbing the equilibrium of the droplet. Heines and Westwater experimentally investigated spontaneous convection, focusing on the effects of lateral temperature variations along the interface, which was brought about by the enthalpy change accompanying solute transfer [8]; however, they experimentally confirmed that no systematic dependency existed between flow appearance and temperature perturbations. They concluded that the surface tension driving force should arise not from temperature perturbations, but from concentration perturbations.

Lewis and Pratt also pointed out that pulsations were apparently associated with a "shock wave" originating within or on the surface of the droplet. The shock wave is regarded as the normal ejection of solute-rich material, called eruption [5]. Eruption is associated with a tangential pulling away of the interfacial layer and normal ejection of solute-rich material. Lewis and Pratt also reported violent circulation at the surface of the droplet when aluminum powder was suspended in the droplet. This indicates that nonturbulent layers adjacent to the interface can be absent under such conditions, and the laminar film model can no longer hold true in this case. Many researchers have experimentally studied the enhancement of the mass transfer rate due to interfacial turbulence. The ratio F of the mass transfer measured as the predicted values from the penetration theory increased by a factor of 1.5 to 4 with increasing driving force (solute concentration) [9–13].

After Lewis's seminal work, theoretical and experimental investigations of spontaneous droplet motion have been undertaken, mainly based on hydrodynamic effects. Haydon and Davies produced oscillation in a pendant droplet of water in toluene by squirting acetone from a capillary on one side of the droplet, and calculated the energy dissipated against viscous forces while damping the oscillations [14,15]. Comparing the dissipation energy with the energy acquired from the change of interfacial tension, they obtained the linear relation between the two energies. They found that oscillation damping, such as kicking or erratic pulsation, arises from a localized change in interfacial tension. Sorensen *et al.* investigated the hydrodynamic and chemical stability of kicking droplets suspended in an infinite amount of another immiscible liquid by the methods of linear hydrodynamic stability theory, and presented the necessary conditions for the system to become unstable [16]; however, the theory is only an initial step towards understanding kicking droplets because the analysis involved an undesirable approximation, equating the size of the system

*Corresponding author; tban@mail.doshisha.ac.jp

with the size of the biological cell membrane.

There are two methods to design directed movement of droplets: use of the change in surface energy of substrates [17–22] and interfacial instability [23–30]. Droplets of reactive solution are placed on partially wettable substrates. Droplets change the wettability of the substrate by adsorption and/or desorption of a solute and the droplet then begins to move along a surface-energy gradient. Ban and co-workers chemically controlled droplet motion using interfacial instability [25–28]. A droplet containing various metal ions formed at the tip of the nozzle in the heptane phase with 5 mM di-2-ethylhexyl phosphoric acid (DEHPA) [25]. The droplet was expanded by a syringe pump at a constant rate. Only the Ca-containing droplet exhibited regular oscillation, whereas the droplet containing other ions grew without oscillation. Periodic eruptions of materials from the droplet were seen during oscillation, inducing internal flow, which was found to be a cause of droplet oscillation. A role of the solution supply was to maintain the system far from equilibrium, leading to the development of internal flow and producing sustained eruptions. Ban and co-workers also experimentally studied droplet motion depending on the hydrophobicity of anionic chemicals in the droplet [26]. When a nitrobenzene droplet containing 100 mM phenyl borate (PB) formed on a glass plate in an aqueous phase containing 1.15 mM trimethylstearylammonium chloride, the droplet moved randomly at almost a constant speed. For a droplet containing 100 mM DEHPA, which is less hydrophobic than PB, the shape repeatedly changed from a hemisphere to flat without translation: it only showed an oscillatory change in the contact angle at the periphery. Inchworm motion of the droplet containing both PB and DEHPA could be seen; the droplet moved with oscillatory change in the shape. The oil and/or water interface mentioned above has high interfacial tension. Thus, the change in surface energy produced by *ad* and/or desorption processes and chemical reactions generated nonzero net force for droplet motion. This mechanism cannot be applied to an aqueous aqueous liquid system such as a living cell because of the extremely low interfacial tension; however, using air and/or water surface energy, Ban and co-workers succeeded in inducing spontaneous motion in two kinds of aqueous two-phase systems, dextran/polyethyleneglycol (PEG), and Na_2SO_4/PEG systems [27]. The droplet phase was saturated with DEHPA using NaOH. When a single droplet formed in PEG solution, the droplet showed slow random walk motion immediately after placement. When approaching the vessel wall, motion accelerated. Once the droplet contacted the wall, it stopped moving. If a droplet was deposited near a random-walking droplet, the droplets approached and finally coalesced. Motion after the deposition of another droplet is almost linear without a random walking nature. For three droplets, the droplets moved toward the center of the droplet group. The droplets seemed to take the shortest route to the meeting point and moved as if recognizing their mutual position. The collective motion of droplets was induced by spontaneous breaking of flow symmetry around the droplets. Toyota and co-workers reported that the formation of giant vesicles near the surface of the oil droplet induced self-propelling movement of the droplet in a direction opposite the trail of the vesicles [29,30]. Circular convection induced by vesicle formation was observed inside the droplet. Its convection is considered the driving force of the movement.

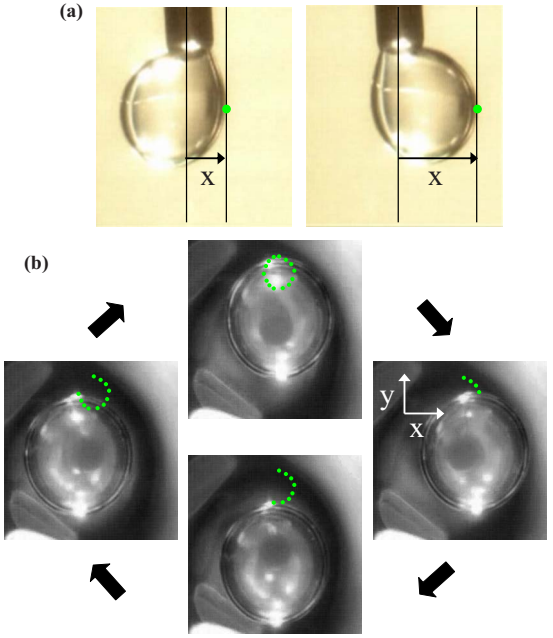

FIG. 1. (Color online) Definition of coordinates of droplet motion in one (a) and two (b) dimensions.

In this way, the spontaneous fluid flow induced by interfacial instability plays an important role in droplet motion and in the enhancement of the rate of mass transfer. In this paper, we showed that interfacial instability induced droplet motion and the motion changed with the solute concentration and volume growth rate of droplet. Furthermore, we revealed that the evolution of droplet motion depends on the flow pattern inside the droplet. Internal flow develops to a vortex pair. In general, when a droplet moves in fluid, the internal flow can become a vortex due to the transfer of momentum from the surrounding media [31,32]. In our study, spontaneously generated internal flow, which is induced by interfacial instability, causes droplet motion. We will discuss the relation between droplet motion and flow pattern.

II. EXPERIMENT

A pendant droplet was formed at the tip of a stainless steel nozzle in a glass vessel. We continuously supplied aqueous solution to the droplet using a syringe pump at a volumetric flow rate ranging from 25 to 100 μL/min. Thus, the droplet kept growing during the experiments. The inner (ID) and outer diameters (OD) of the nozzle were 1.2 mm and 1.6 mm, respectively. The glass vessel was immersed in a water bath with a thermostat accurate to within ± 0.5 °C and we varied the temperature between 15–35 °C. We used toluene, heptane, and decane as the organic phase, and acetone as the solute varied in concentration between 0.4 and 10.0 vol %. Acetone was added to the water or organic phase to investigate the effect of the direction of mass transfer on droplet motion. Figure 1 illustrates our definition of coordi-

nates of droplet motion in one and two dimensions. Figure 1(a) shows snap shots of droplet motion from the side view. The z axis is parallel to the nozzle. Most droplet motion was confined in a horizontal plane perpendicular to the z axis. Thus, we took the x coordinate of a point on the outer contact surface of the droplet from the origin to analyze droplet motion. Figure 1(b) shows snap shots of droplet motion from the bottom view. We recorded the trajectory of a point on the droplet surface. There was no significant change in the oscillation pattern of a droplet among different variables describing droplet motion, such as the inclined angle of the central meridian of the droplet to the z axis and the selection of observation points in the droplet. We defined time zero as when the droplet grew larger than the outer diameter of the nozzle. Measurements were performed until the droplet separated from the nozzle. Droplet motion was recorded by a high-speed video camera (FASTCAM-PCI R2, Photron) from the side or bottom of the vessel and was analyzed by image analysis software (Movie Ruler, Photron). We colored the organic phase surrounding the droplet with iodine to visualize mass transfer, and added silica powder to the droplets to visualize the internal flow pattern.

Equilibrium and dynamic interfacial tension were measured by the droplet weight method and pendant droplet method, respectively. The experimental procedure of equilibrium interfacial tension is described elsewhere [23]. To measure dynamic interfacial tension, a water droplet containing 5 vol % acetone was formed at a volumetric flow rate of $V=250\ \mu$L/min. When the neck of the droplet had formed, solution supply was stopped. We then estimated dynamic interfacial tension from the change in droplet shape during mass transfer of acetone from the droplet to the surrounding media.

III. RESULTS

A. Droplet motion

When two driving forces, mass transfer of acetone and a constant flow of solution supply, are imposed on the pendant droplet, flow inside the droplet develops spontaneously and the droplet begins to move. Droplet motion depends on acetone concentration in the droplet phase, C, and the volumetric flow rate of the solution supply, V. For $C \leqslant 0.4$ vol %, internal flow did not develop and the droplet showed no oscillation. As the acetone concentration increased beyond a critical value, hierarchical changes in dissipative structures of the flow pattern inside a droplet, mass transfer behavior, and droplet motion were observed. Figure 2 shows the typical sustained motion of a droplet with $C=2$ vol % at different flow rates. For $V=25\ \mu$L/min, the long wave pattern of droplet motion is shown in Fig. 2(a). Fast oscillation develops at about 110 sec. For $V=50\ \mu$L/min, we can see that droplet motion progresses in well-defined stages in Fig. 2(b). Motion develops in three stages. The lower panels in Fig. 2(b) show two-dimensional motion of the droplet from the bottom of the vessel. In the first stage, the droplet turns very slowly on the nozzle, and wiggles with small amplitude, as shown in panel (a) of Fig. 2(b). Phase difference between Y and X components of displacement in slow oscillation in

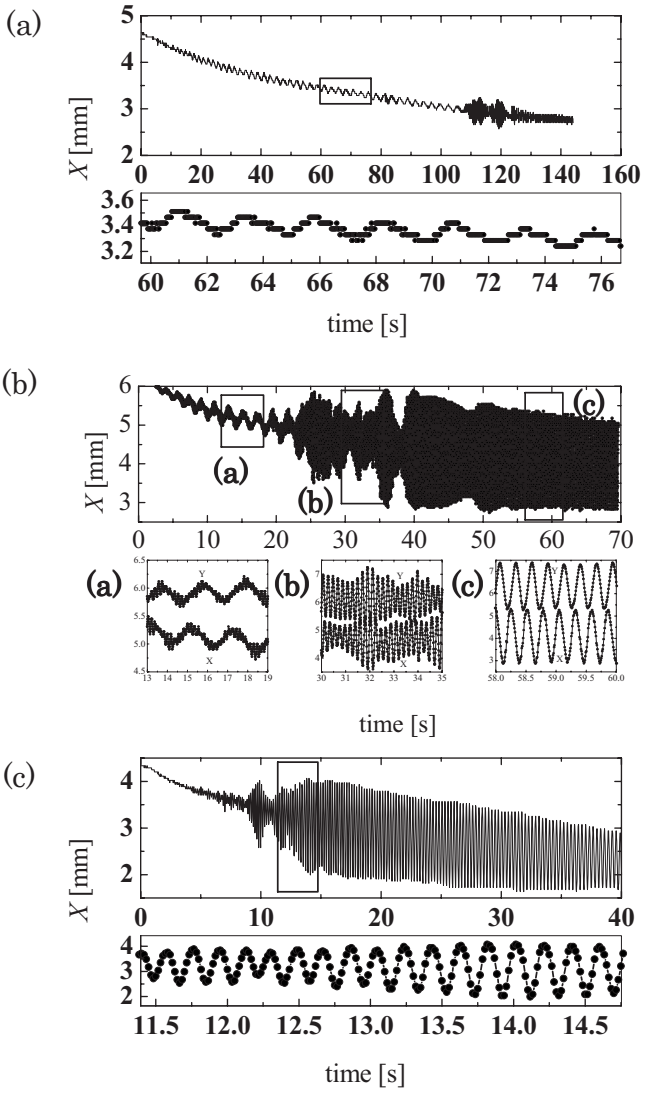

FIG. 2. Evolution of droplet motion at different volumetric flow rates, (a) $V=25\ \mu$l/min, (b) $V=50\ \mu$l/min, and (c) $V=100\ \mu$l/min. Water droplet containing 2 vol % acetone was formed at the stainless steel nozzle, 1.2 mm inner diameter, in toluene at room temperature. Lower panels are an expansion of the box in upper panels. Lower panels in (B) represent two-dimensional motion of the droplet in the first stage (a), second stage (b), and third stage (c).

panel (a) of Fig. 2(b) is one-quarter wavelength, indicating that droplet motion is rotational. The wiggle is simple harmonic oscillation because the phase difference is negligible or a half wavelength. In the second stage, the droplet exhibits random pendulum or rotational motion, as shown in panel (b) of Fig. 2(b); the oscillation amplitude changes randomly. In the third stage, quick regular rotation appears in panel (c) of Fig. 2(b). Amplitude and frequency of the rotation in the third stage are almost constant and about ten times larger than in the first stage. For $V=100\ \mu$L/min, fast rotation occurs in the induction period a few seconds after droplet formation. Change in the motion modes of droplets with different flow rates could be reproduced very well. The average deviation of the period and amplitude of oscillations is within 15% in each measurement. We carried out experi-

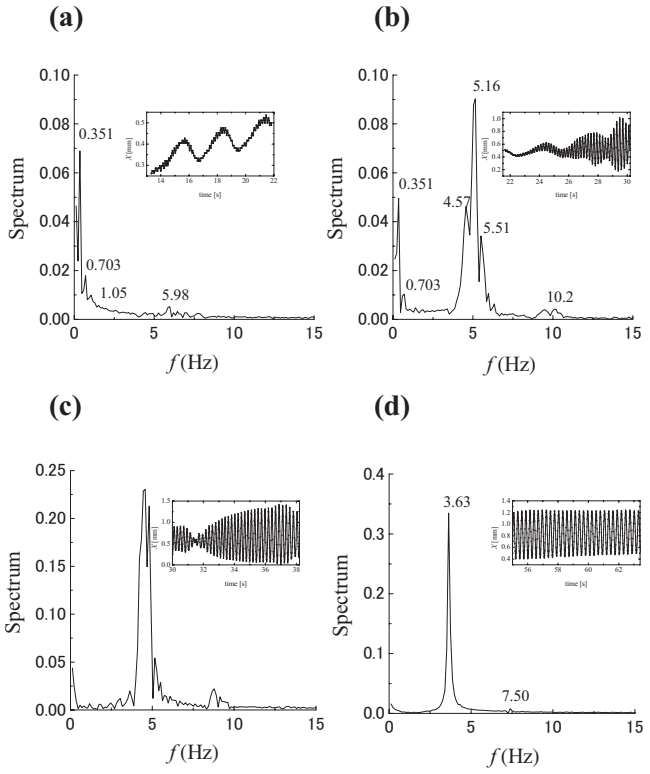

FIG. 3. Evolution of droplet motion and the corresponding frequency spectra when droplet motion develops hierarchically at $C=2$ vol % at $V=50$ μL/min. Frequency spectra correspond to the oscillation patterns of the insets. Numbers in figures are frequency values at peaks. (a) First stage of droplet motion, (b) transition state from the first to second stage, (c) second stage, (d) third stage.

ments with temperature changes and found no substantial change in droplet motion within the temperature range from 15 to 35 °C.

The droplet with $C=2$ vol % at $V=50$ μL/min showed the onset, transition state, and stable state in dissipative structures; therefore, we focused on the system and discuss droplet motion in detail. Figure 3 shows the evolution of oscillation patterns and the corresponding frequency spectra when droplet motion develops through these three stages. At the beginning of droplet growth, a peak appears at low frequency, corresponding to the long wave in the first stage of droplet motion, and the second and third harmonics of the wave are observed in Fig. 3(a). A small peak is observed around 6 Hz, corresponding to the wiggle in the first stage. As the droplet grows, this peak becomes higher, and splits into three well-defined peaks, as shown in Fig. 3(b). The frequency of the middle peak is almost equal to the arithmetic mean of the higher and lower values. The three peaks then become broad and unify, as shown in Fig. 3(c). Many small peaks appear around the highest peak and, in this case, the droplet exhibits random oscillation corresponding to the second stage. As the droplet grows further, small peaks disappear and the highest peak develops to a monochromatic wave, as shown in Fig. 3(d). Here we can see regular rotation, corresponding to the third stage. The unified peak becomes sharp and the second harmonic of the peak appears.

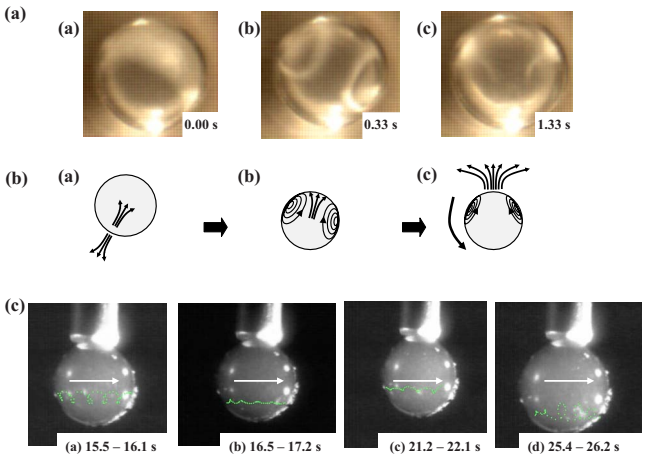

FIG. 4. (Color online) Evolution of self-organized flow and mass transfer in the first stage at $C=2$ vol % at $V=50$ μL/min. (a) A vortex pair from bottom of the vessel. (a) Internal flow induced by solute eruption, (b) onset of a vortex pair, and (c) thinning of the vortex pair. Number in panels is time from onset. (b) Corresponding mass transfer. (a) Eruption and irruption are generated, (b) irruption strikes the opposite side of the initial generation point directly, and (c) eruption occurs from the vortex pair. (c) Trajectory of vortex center from side view when the vortex pair rotates unidirectionally. (a) Loop pattern, (b) smooth pattern, (c) cusp pattern, and (d) amplitude modulation. See movie [33].

B. Flow pattern and mass transfer

To investigate the cause of mode change in droplet motion at $C=2$ vol % and $V=50$ μL/min, we observed the development of the flow pattern inside the droplet and mass transfer. Internal flow from the bottom view in the first stage is shown in Fig. 4(a). Silica powder captures the flow patterns inside the droplet. Illustrations in Fig. 4(b) represent mass transfer behavior corresponding to the development of internal flow, as shown in Fig. 4(a). First, a jetlike flow erupts out of the droplet, as described in Fig. 4[(B)a]. The flow reaches several times the size of the droplet and is considered to be the eruption of acetone-rich material. Goltz reported that schlieren photographs showed direct evidence of this eruption [5] and Komasawa showed that, in the same system, the mass transfer rate of acetone increased by 2.1–2.3 times due to eruption [12]. The eruption is simultaneously generated inside the droplet, and the flow strikes the opposite side of the initial generation point directly. The resulting internal flow develops along the interface of the droplet and then divides into a counter-rotating pair of vortices, as shown in panels (b) of Fig. 4(a) and 4(b). Subsequently, the vortex pair thins and is confined to the thin spherical shell of the droplet near the interface in panel (c) of Fig. 4(a). The vortex pair in our system had a different configuration from the normal vortex pair, which is aligned in the horizontal plane. Our vortex pair, which was confined to the superficial layer of the droplet, rose almost vertically and was present on each side of the droplet. The planes where vortices occur are parallel to the droplet surface; therefore, the vortices are not a continuously closed vortex ring. Their configuration resembles two wheels connected to a shaft (see movie [33]). The droplet has

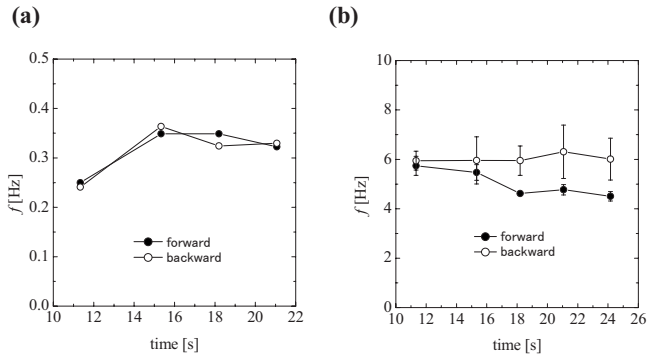

FIG. 5. (a) Precessional frequency and (b) nutational frequency of the vortex pair in the first stage of droplet motion for $C=2$ vol % at $V=50$ μL/min. Open and closed keys are the periods of back- and forward-rolling vortices, respectively.

the combined structure of bulk and a thin superficial layer. The flow in the bulk is different from the superficial layer and has a complicated pattern that could not be analyzed. As the vortices developed, continuous eruptions occurred on the opposite side of the initial point from the vortices into the surrounding media, as illustrated in Fig. 4[B(c)]. As the droplet grew bigger, the vortex pair moved right and left. The pair then rotated clockwise or anticlockwise along the interface with a constant distance between the vortices. The direction changed in the early stage after droplet formation. After the induction period, the motion of the vortex pair settled into unidirectional rotation, with continuous eruptions encircling the droplet with vortex rotation. Figure 4(c) describes the trajectory of the vortex center from the side view when the vortex pair rotated unidirectionally. The number in Fig. 4(c) represents the time taken for the vortex to pass through one side of the droplet. The vortex rotated about the axis of the nozzles with oscillation. The path of the vortex changed with time and traced a loop, a smooth or cusp curve trajectory. Its motion appeared similar to the precession of a spinning top accompanied by nutation. Panel (a) of Fig. 4(c) shows the loop pattern of the forward-rolling vortex. Subsequently, we could see the smooth pattern of the back-rolling vortex on the right side of the droplet shown in panel (b) of Fig. 4(c) and the cusp pattern of the forward-rolling vortex in panel (c) of Fig. 4(c) As the droplet grew bigger, amplitude modulation of the nutation was observed, as in panel (d) of Fig. 4(c). The center of the vortex exhibited a beatlike pattern.

Figure 5 shows the frequencies of the precession and nutation of each vortex in the first stage at $C=2$ vol % at $V=50$ μL/min; precessional frequency of the two vortices was almost the same, with the vortices becoming slightly different in nutational frequency over time. Nutational frequency of the forward-rolling vortex decreased gradually, whereas that of the backward-rolling vortex maintained a constant value.

Vortex motion and mass transfer behavior in the second and third stages are illustrated in Fig. 6. After amplitude modulation, the two vortices moved randomly, as shown in the left and middle panels of Fig. 6(a). The vortices interacted with each other, and then collapsed gradually as the

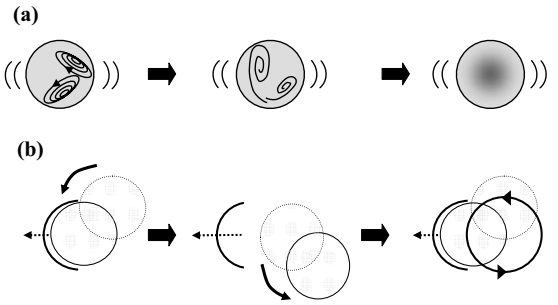

FIG. 6. Illustration of self-organized flow and mass transfer behavior from bottom of the vessel in the second (a) and third stages (b) at $C=2$ vol % at $V=50$ μL/min. (a) The vortices interact and then collapse gradually as the droplet grows. Solute eruptions occur many times randomly all over the droplet surface in the second stage. (b) Spherical compression waves extend radially from the droplet surface. The droplet emitted one pulse of mass transfer for each revolution of the droplet.

droplet grew. Vortex motion corresponded to the second stage of droplet motion, as shown in panel (b) of Fig. 2(b). Finally, the two vortices merged and disappeared, as shown in the right panel of Fig. 6(a), leading to the third stage of droplet motion. During the third stage, spherical compression waves appeared at a certain point on the droplet surface from the bottom view and extended radially, as illustrated in Fig. 6(b). Spherical waves were observed as the propagation of a circular curve corresponding to changes in the refractive index. The spherical waves could be considered as solute eruptions condensed into a spherical wave pattern. In this stage, the side view of the droplet showed that silica powder near the interface drifted from the "equator" to the "south pole" of the droplet and returned to the starting point.

Figure 7 shows the relation between vortex dynamics and droplet motion for $C=2$ vol % at $V=50$ μL/min. The period of slow rotation in the first stage of droplet motion and the average precessional period of the vortex pair are shown in Fig. 7(a); both periods have almost the same value. Figure 7(b) shows the time evolution of x coordinates in droplet

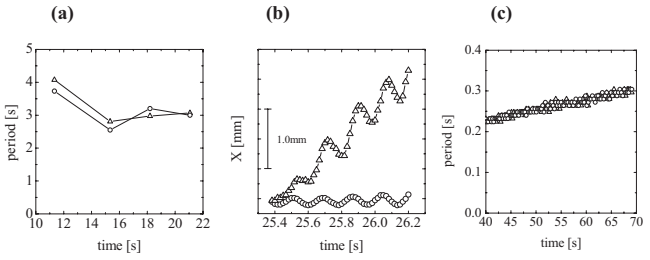

FIG. 7. (a) Rotational periods of droplet (circular key) and average precessional period of the vortex pair (triangular key) in the first stage of droplet motion at $C=2$ vol % at $V=50$ μL/min. (b) Time evolution of x coordinates in wiggle motion of the droplet and the corresponding motion of the vortex shown in Fig. 4 [(C)d]. Motion of the droplet and vortex are represented by circular and triangular keys, respectively. (c) Period of fast rotation of the droplet and period of spherical compression waves in the third stage. Periods of droplet motion and spherical compression waves are represented by circular and triangular keys, respectively.

wiggle in the first stage and the corresponding motion of the vortex shown in Fig. 4[(C)d]. The motion of the droplet is synchronized with that of the vortex. In the second stage, we could not analyze the motion of the vortices because they exhibited random and complex motion. Random motion of the droplet, shown in Fig. 2[(B)b], was observed until the two vortices merged. Figure 6(c) shows the period of fast rotation of the droplet and the occurrence period of spherical compression waves in the third stage. The time taken for one revolution of the droplet is almost equal to the occurrence period of spherical compression waves. The droplet emitted a circular wave pulse for each circular motion of the droplet.

We investigated flow patterns inside the droplet for $C=2$ vol % at $V=25$ and 100 μL/min (data not shown). For $V=25$ μL/min, precessional motion of vortices was observed. When the droplet exhibited a long wave pattern, as shown in Fig. 2(a), the rotational axis of the vortices was stable and no nutation was observed. The vortex center fluctuated 110 sec after droplet formation. In this case, droplet motion was disturbed in response to vortex motion. For $V=100$ μL/min, we observed that, just after droplet formation, a vortex was generated but suddenly broke up. Internal flow then followed the flow pattern in the third stage of droplet motion at $V=50$ μL/min.

C. Necessary factors for droplet motion

To study the factors necessary for droplet motion, we investigated each effect of the two driving forces, mass transfer, and solution supply. When a droplet without acetone formed at a constant growing rate, the droplet steadily grew bigger without oscillation and organized flow inside the droplet was not observed. Next, we carried out experiments using a droplet with 2 vol % acetone without solution supply. The droplet developed to a certain size and then solution supply was stopped. In this case, we found that the droplet did not move and acetone eruptions occurred at almost the same point on the interface at regular intervals. The period of eruption for a droplet of 3 mm diameter containing 2 vol % acetone was 4.3 ± 0.2 sec and that for a droplet of 5 mm diameter was 3.8 ± 0.1 sec. Internal flow was generated whenever eruptions occurred; however, the flow quickly subsided before it developed a vortex pair.

We investigated the effect of the linear velocity of solution supply on droplet motion. A droplet was formed using a large nozzle, 2.5×3.0 mm inner and outer diameters at $V=25$ μL/min. Thus, the linear velocity of the solution introduced from the nozzle tip was slower than in Fig. 2, in which droplets were formed using a nozzle of 1.2×1.6 mm diameter. This result is shown in Fig. 8. With the large nozzle, oscillation was erratic and intermittent. The droplet showed kicking after an incubation period without sustained oscillation. When the solution supply rate was too slow, sustained droplet motion did not occur.

We investigated the effect of the direction of mass transfer and solution supply on droplet motion. Figure 9(a) shows the typical behavior of a pure water droplet in toluene phase containing 2 vol % acetone; mass transfer occurs in the opposite direction. When the direction of mass transfer was

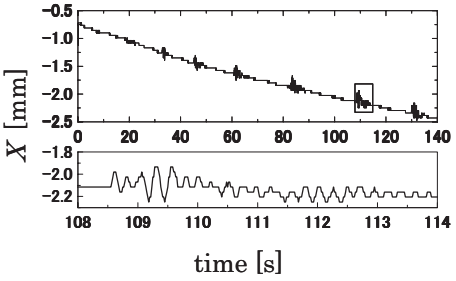

FIG. 8. Evolution of droplet motion at $V=25$ μl/min. A droplet containing 2 vol % acetone was formed at the stainless steel nozzle, 2.5 mm inner diameter, in toluene at room temperature. Lower panels are an expansion of the box in upper panels.

from the surrounding media into the droplet, only erratic motion of the droplet with small amplitude was observed; the internal flow did not develop to a vortex. Figure 9(b) shows the effect of solution supply on an oscillating droplet. When we stopped supplying solution to the oscillating droplet during mass transfer from the droplet to the surrounding media, droplet motion ceased. When solution supply was restarted, regular oscillation of the droplet occurred again.

As described in Sec. III A, we have shown the experimental results in a system where a water droplet formed in the organic phase. Next, we carried out an experiment with the

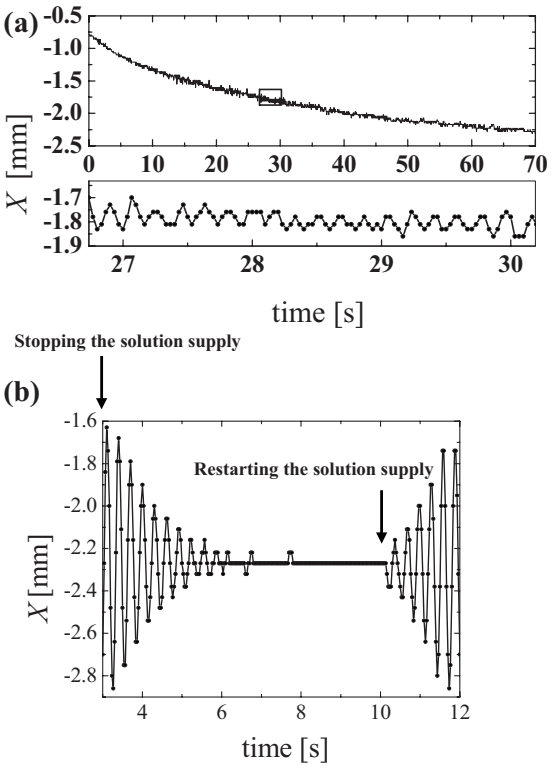

FIG. 9. Effect of the direction of mass transfer and solution supply on droplet motion. (a) Droplet motion when the direction of mass transfer occurs from the surrounding media into the droplet. Surrounding media contains 2 vol % acetone. (b) Effect of on-off supply of solution to the droplet on droplet motion in the third stage. Left arrow indicates the time of stopping solution supply, and the right arrow the time of restarting solution supply.

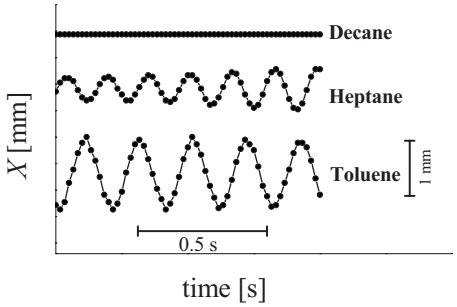

FIG. 10. Droplet motion in different organic solvents with 5 vol % acetone at $V=25$ μl/min.

opposite arrangement, using a toluene droplet containing 2 vol % acetone in a water phase at a flow rate of 50 μL/min. We found that the droplet exhibited similar motion, as shown in Fig. 2(b) (data not shown).

The above results show that droplet motion requires two conditions, mass transfer from a droplet to the continuous phase and droplet growth. Spontaneous eruption produces a vortex pair inside the droplet, and droplet growth maintains vortex pair motion without attenuation; the vortex pair induces droplet motion. Next, we investigated the cause of the onset of eruption. We performed these experiments with other organic solutions, heptane and decane, with 5 vol % acetone. Typical motion of the droplets is shown in Fig. 10. When we used heptane as the organic phase, droplet motion was similar to that in the toluene system. Oscillation amplitude in the heptane system is smaller than in the toluene system. The decane system, however, does not show any oscillation. Periodic eruptions were observed in the heptane system, whereas eruptions were not seen in the decane system.

Interfacial tension was measured under equilibrium and nonequilibrium. Figure 11(a) shows equilibrium interfacial tension with three organic solvents, toluene, heptane, and decane. The concentration in the figure means acetone concentration in the organic phase at equilibrium. The equilibrated acetone concentration in all systems was determined from the distribution coefficient of acetone between toluene and water [34]. Equilibrium interfacial tension in all systems decreases monotonically by increasing acetone concentration. We measured dynamic interfacial tension using the pendant droplet method. A water droplet containing 5 vol % acetone was formed at a volumetric flow rate of $V=250$ μL/min. When the neck of the droplet had formed, solution supply was stopped. We then estimated dynamic interfacial tension from the change in droplet shape during mass transfer of acetone from the droplet to the surrounding media. Without solution supply, the droplet cannot oscillate. Figure 11(b) shows dynamic interfacial tension during mass transfer. Toluene and heptane systems showed an increase in dynamic interfacial tension over time, whereas the decane system showed no change in dynamic interfacial tension during measurements; however, the absolute value of dynamic interfacial tension in the toluene system is much higher than the equilibrium value. Experimental accuracy in the toluene system is not so high as that in the heptane and decane systems because the droplet neck in the toluene system was not created due to affinity to the surface of the nozzle. The nozzle is more wettable with toluene than heptane and decane and can therefore cause experimental errors in the toluene system; however, the most important aspect is the changed behavior of dynamic interfacial tension rather than the absolute value. In particular, for the toluene system, the amount of change in dynamic interfacial tension is largest among the three systems. The amplitude of droplet oscillation increases with the increased change in dynamic interfacial tension, as shown in Fig. 10. It should be noted that the usual dynamic interfacial tension decreases with time because the amount of surfactant adsorbed at the interface increases with time [35]. The behavior of dynamic interfacial tension in our systems is considerably different from the usual surfactant system. We will discuss the mechanism in the next section, demonstrating that this behavior causes eruption.

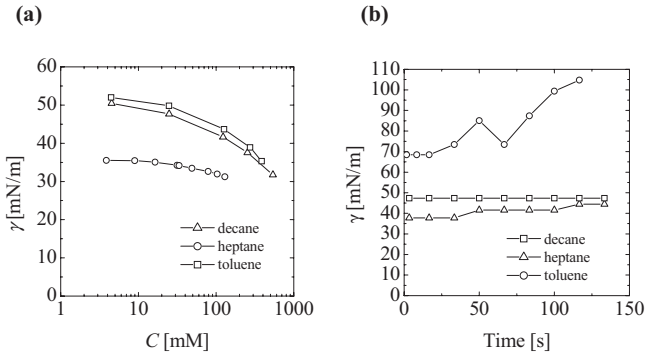

FIG. 11. (a) Equilibrium interfacial tension of the three systems, water toluene, heptane, and decane, against acetone concentration at 25 °C. Concentration, C, means equilibrium acetone concentration, which is determined from the distribution coefficient of acetone between toluene and water [34]. (b) Dynamic interfacial tension behavior of water droplet containing 5 vol % acetone in the three systems, toluene, heptane, and decane at 25 °C.

IV. DISCUSSION

We have reported that spontaneous motion of the droplet and self-organized flow inside the droplet develop hierarchically with solute eruptions during droplet growth. We have found that droplet motion changes with the solution supply rate and the development of internal flow controls droplet motion. Understanding the mechanism of internal flow development will shed light on the mechanism of the occurrence and development of droplet motion. At $C=2$ vol % at $V=50$ μL/min, droplets showed the three patterns of droplet motion and internal flow shown in Fig. 2, whereas at $C=2$ vol % at $V=25$ and 50 μL/min, one type of droplet motion was observed; therefore, we focused on droplet motion at $C=2$ vol % at $V=50$ μL/min and discuss the development of internal flow, which is summarized as follows:

(1) Onset of eruption.
(2) Sustainability of a vortex pair.
(3) Precession and nutation of the vortex pair.
(4) Interaction of the vortex pair.

A. Onset of eruption

Eruption is a crucial trigger of the sequence of internal flow. Without eruption, internal flow does not occur and the droplet does not move. Transport phenomena of the solute to an interface are involved in the onset of eruption. There are two ways to develop spontaneous fluid flow: cellular convection and eruption. Cellular convection was first studied by Sternling and Scriven [3,4], and Sawistowski proposed the necessary condition for the onset of eruptions in view of the change in dynamic interfacial tension [6]. Initially, inhomogeneous concentration distribution due to a certain uncontrollable perturbation forms at the interface. The area with the highest concentration will expand outward due to the interfacial tension gradient. If solute-rich material is supplied from bulk to the affected area by the induced convection, the concentration in this area will further increase and then outward expansion will be enhanced. Finally, fluid flow develops to a convection cell. If solute-poor instead of solute-rich material is supplied to the affected area, interfacial tension at the center of the affected area will increase. Consequently, the direction of fluid flow will be reversed and inward flow will occur. The resulting inward flow will produce a jetlike ejection which is normal to the interface. Jetlike ejection to the surrounding medium is called eruption and that into the droplet is called irruption; this is the Sawistowski model [6]. If the flow induced by irruption is squirted onto a curved surface, it may grow into a vortex pair. When a system follows the Sawistowski model, a vortex pair may generate. The Sawistowski model, however, has the fatal problem that infinitesimal perturbation never induces macroscopically developed flow. Even though solute-poor material moves into the affected area, the expanded area recovers without eruptions because the resulting inward flow counteracts flow from the bulk. In the Sternling and Scriven model, expanded flow can develop to macroscopic flow, such as cellular convection, because expanded flow promotes solution supply from the bulk and vice versa. Unless macroscopic conditions are inherent at the interface, eruptions do not occur at the interface. One of these conditions is considered to be the formation of a solute-rich macroscopic layer at the interface. If the macroscopic layer is formed at the interface and then solute-poor material moves into this layer, interfacial tension in the area will increase and inward flow will occur to compress the area, resulting in eruptions. Such formation of the macroscopic layer can be seen when a large amount of evaporated volatile solvent is supplied to the surface of a less volatile solvent [36]. A less volatile organic solvent, e.g., toluene, is poured into a cylindrical vessel, and a more volatile solvent, e.g., pentane, is placed around the vessel. The volatile solvent evaporates and is adsorbed onto the surface of the less volatile solvent. Inhomogeneity in surface tension induces spontaneous surface flow due to the Marangoni effect. At the beginning of the experiment, surface flow appears random. As mass transport continues, regulated solitary waves appear. In this case, a macroscopic pentane-rich layer transiently forms on the toluene surface. Pentane accumulates on the toluene surface because the dissolution rate cannot keep up with the solvent supply. A similar situation can occur on the droplet surface in our system if acetone concentration in the droplet is sufficiently high. After an acetone-rich layer forms macroscopically at the droplet interface, and if solute-poor material is supplied from bulk to the solute-rich macroscopic layer by solution supply, the interface can satisfy the condition to induce eruption. The experimental result shown in Fig. 11(b), in which dynamic interfacial tension increases over time, supports the formation of the acetone-rich macroscopic layer. The result indicates that the acetone-rich layer is formed in the early stage and then acetone gradually passes across the interface. The increase in dynamic interfacial tension with time can result from the difference between the rates at which the solute reaches and subsequently leaves the interface. When solute concentration is higher than the critical value, a rate difference occurs and induces solute accumulation at the interface, which develops a solute-rich macroscopic layer. The resulting interfacial instability induces eruption and irruption, and in turn irruption generates a vortex pair on the droplet surface.

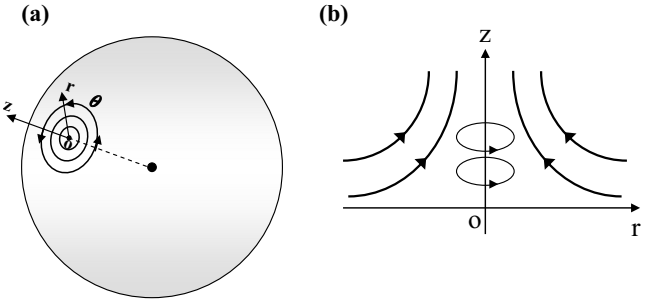

FIG. 12. Schematic representation of vortex confined to the spherical shell of the droplet. (a) Cylindrical coordinates on the surface. (b) Axial symmetry stretching flow.

B. Sustainability of a vortex pair

We will now consider why the vortex pair continues to move without attenuation. The vortex in the present study is considered to be a two-dimensional circular vortex because it is confined to the thin spherical shell of the droplet. In general, vortex motion in a viscous incompressible fluid is governed by an equation analogous to the diffusion equation. Thus, vortex motion decays over time due to viscous force. The attenuating motion corresponds to vortex motion in the present experimental systems when the droplet contains 2 vol % acetone without solution supply or a droplet is formed using a large nozzle, 2.5 mm inner diameter at $V=25\ \mu\mathrm{L/min}$, shown in Fig. 8. In this case, transient internal flow appeared and quickly decayed. Without solution supply or at a slow rate, the vortex collapsed. For a growing droplet, the vortex maintained its shape and continued to move without decaying. Solution supply plays an important role in sustained motion of the vortex. The role of solution supply can be described as follows. The growth direction of the droplet is normal at the droplet surface; therefore, we consider that flow near the interface serves as axisymmetric stretching flow in the growth direction. Schematic representations of the vortex confined to the spherical shell of the droplet and axisymmetric stretching flow are illustrated in Fig. 12. Hence, axisymmetric stretching flow represents v

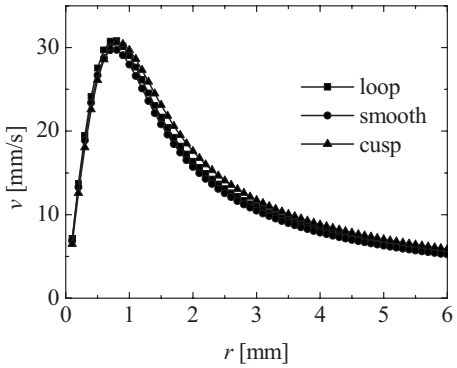

FIG. 13. Velocity profile of vortices in the three patterns. Curves are calculated by substituting the experimental values, α and ω_o, shown in Table I, in Eq. (3).

$=[-1/2\alpha r, v(r,t), \alpha z]$ in cylindrical coordinates. We obtained the equation of vortex motion, $\boldsymbol{\omega}=(0,0,\omega)$,

$$\frac{\partial \omega}{\partial t} - \frac{\alpha}{2r}\frac{\partial}{\partial r}(r^2\omega) = \nu\left(\frac{\partial^2 \omega}{\partial r^2} + \frac{1}{r}\frac{\partial \omega}{\partial r}\right), \tag{1}$$

where ν is kinematic viscosity. In the steady state, we have

$$\omega(r) = \omega_0 \exp\left(-\frac{\alpha}{4\nu}r^2\right), \tag{2}$$

where ω_0 is vorticity at the central axis of the vortex, and

$$v(r) = \frac{2\nu\omega_0}{\alpha r}\left\{1 - \exp\left(\frac{-\alpha}{4\nu}r^2\right)\right\}. \tag{3}$$

This vortex is called a Burgers vortex [37,38]. The velocity profile of Eq. (3) is shown in Fig. 13. The velocity profile of the Burgers vortex near the axis is proportional to r, indicating that, in this range, the vortex behaves as rigid body rotation with constant angular velocity [38,39]. A steady vortex is maintained by balancing the increase in vorticity due to stretching of the vortex and attenuation of vorticity by drag force. The curves in the figure represent the velocity profiles of the vortex in the three pattern of vortex motion. The values of ω_0 and α in the three patterns are calculated from the experimental results, and the calculation method will be explained in the next section. In our experimental systems, the stretching rate, α, depends not on the volume growth rate of the droplet, but on the linear velocity of the solution introduced from the nozzle tip because even at the same volume growth rate, droplet motion depends on the nozzle diameter, as shown in Figs. 2(a) and 8. As shown in Fig. 8, for the slowest linear velocity, intermittent droplet motion occurs. Although the droplet contains 2 vol % acetone, the linear velocity, however, is insufficient to keep the velocity profile of the generated vortices steady; thus, the vortices quickly decay. When linear velocity is increased beyond the value at which stretching flow can maintain the steady velocity profile of the vortex, the vortex can move without attenuation and droplet motion can be sustained. The sustainability of the vortex requires two effects: sufficiently high acetone concentration and linear velocity of the solution supply. Changes in droplet motion are induced by other mechanisms. We will discuss this mechanism in the next sections.

C. Precession and nutation of the vortex pair

When experimental conditions satisfied the two requirements described above, a vortex pair could maintain a steady velocity profile. The vortex pair requires different factors for movement. As described in the results of Fig. 4, in the early stage of vortex pair formation, the vortex pair did not move and then swayed slightly from side to side. The pair then rotated clockwise or anticlockwise along the interface with a constant distance between the vortices. Why does precession occur? Velocity induced by a vortex controls the motion of another vortex [38,39]. In general, when a vortex pair has the same strength, it travels in a straight line. Thus, the vortex pair in the droplet does not move because the traveling direction is normal to the droplet surface. When a vortex pair has different strengths, they rotate on the centroid, divided externally. If either of the vortices in the droplet changes in strength, the vortices begin to rotate. A change in strength may occur due to dissipation of vortex energy to complicated flow in the bulk or interaction between the vortices. The vortex pair, however, rotates not around an externally dividing point, but around an internally dividing point because vortex motion is confined to inside the droplet; therefore, the centroid of the vortex pair deviates from the center of the nozzle. As a result, the vortex pushes the droplet outward and the trajectory of the moving droplet passes through a larger curve than the droplet surface at rest. This explains the slow rotation of droplet motion in the first stage, shown in panel (a) of Fig. 2(b).

Next, we consider nutation of the vortex. According to Eq. (3), the vortex in our experiments can be treated as a rotating cylinder. Assuming that the vortex has a mass different from that of the surrounding media, vortex motion is similar to the behavior of a horizontally propagating cylinder rotating under gravity. The motion equation is given by [38,39]

$$(M + M')\ddot{z} = i\rho\Gamma\dot{z} - i(M - M')g. \tag{4}$$

The solution is

$$z = z_o + Re^{i\Omega t} + Vt, \tag{5}$$

where

$$\Omega = \frac{\rho\Gamma}{M + M'}, \quad V = \frac{M - M'}{\rho\Gamma}g. \tag{6}$$

M and M' are the cylinder and induced mass $(=\rho\pi a^2)$, respectively, z $(=x+iy)$ complex coordinate of the cylinder center, z_o initial position of the cylinder center, ρ density of the surrounding media, a radius of the cylinder, Γ circulation, and g gravitational acceleration. We took the y axis as the direction of gravity. This is called Phugoid motion and uniform circular motion is superimposed on uniform linear motion, resembling a simplified airplane loop. The motion depends on the magnitude relation between V and $R\Omega$. For V less than $R\Omega$, the motion pattern is trochoid (loop). For V to

TABLE I. Vortex characteristics of the three patterns.

Pattern	R (mm)	Ω (rad/s)	$R\Omega$ (mm/s)	V (mm/s)	ρ_v/ρ (−)	ω_o (rad/s)
Loop	0.1875	34.3	6.43	3.06	1.02	69.3
Smooth	0.0278	33.3	0.926	2.93	1.02	67.3
Cusp	0.0865	31.4	2.72	3.02	1.02	63.4
Pattern	d (mm)	Γ (mm^2/s)	α (s^{-1})	$V_{\text{calc.}}$ (mm/s)		
Loop	2.68	51.5	10.8	3.04		
Smooth	2.68	49.4	11.0	2.91		
Cush	2.92	55.3	9.2	3.03		

equal $R\Omega$, the pattern is cycloid (cusp). For V greater than $R\Omega$, the pattern is a wave form (smooth). We consider that V in Eq. (5) corresponds to precessional velocity of the vortex in our experiment, that R in Eq. (5) corresponds to the nutational amplitude of the vortex in our experiment, and that Ω in Eq. (5) equals the angular velocity of nutation. Hence, M and a in the model correspond to the "vortex mass" and radius of the vortex, respectively. On the basis of these assumptions, the values of V and $R\Omega$ in each pattern of vortex motion are summarized in Table I. The relation between V and $R\Omega$ in Table I satisfies the magnitude relation in Phugoid motion; in the case of loop motion, $V<R\Omega$, in the case of smooth motion, $V>R\Omega$, and in the case of cusp motion, $V \approx R\Omega$. The experimental values of V, R, and Ω in the three patterns are substituted into Eq. (5), and the initial condition, z_o, was chosen to fit the trajectory of the three patterns of vortex motion shown in Fig. 4[(C)a]–4[(C)c]. These calculated curves are drawn in Fig. 14. The curves reproduce the three patterns of vortex motion, indicating that this model is valid to elucidate the experimental results. This explains the droplet wiggle in the first stage, shown in Fig. 2[(B)a].

Here, we will calculate the circulation of the vortex, Γ, and the vortex mass. If $r>a$, $\Gamma=\pi a^2\omega_o$; therefore, we use Eq. (6) and $M=\rho_v \pi a^2$, where ρ_v is the vortex density, to calculate ρ_v and ω_o for each motion of the vortex. In addition, vortex circulation bears the following relation to precessional velocity: $\Gamma=2\pi dV$, where d is the distance between the vortex pair; hence, we can calculate the circulation. The calculated values are given in Table I. We found that the vortex is heavier than the surrounding media by 2%; the cause is considered to be as follows. The fluid in the superficial layer, except for the portion of vortex, may be composed of a mixture of water and toluene due to the solubilization effect by acetone. On the other hand, the vortex is mainly composed of water because circulating flow of the vortex itself may repel the penetration of toluene; therefore, the vortex has a mass different from that of the surrounding media.

Here, using Eq. (3), we calculated the circulation round an arbitrary closed curve and found that

$$\Gamma = \frac{4\pi\nu\omega_o}{\alpha}. \tag{7}$$

The stretching rate, α, is calculated from this equation and we obtained the velocity profile of the vortices in the three patterns; the profile is given in Fig. 13. From the velocity profiles, we can calculate precessional velocity, $V_{\text{calc.}}$, by substituting the values of the droplet diameter, which corresponds to the distance between the vortex pair, in Eq. (3). The results are summarized in Table I. Our model provides good agreement between the calculated and experimental values.

D. Interaction of the vortex pair

As explained above, we have understood the mechanism of precession and nutation of the vortex. Vigorous fast rotation of the droplet as seen in the third stage is discussed here.

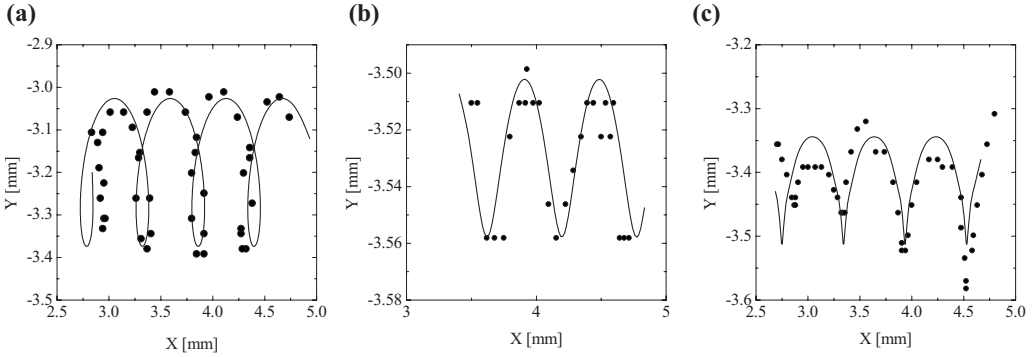

FIG. 14. Comparison between the calculated and experimental values of vortex motion, (a) loop motion, (b) smooth motion, and (c) cusp motion. The experimental values of V, R, and Ω in the three patterns are substituted into Eq. (5), and initial condition, z_o is suitably chosen to fit the trajectory of the three patterns of vortex motion shown in Fig. 4[(C)a]–4[(C)c].

TABLE II. Oscillation characteristics of the vortex pair and the droplet in the transition state from the first to second stage. $f_{\mathrm{low},i}$ and $f_{\mathrm{high},i}$ are lower and higher frequencies of droplet motion at the peaks of the frequency spectrum in Fig. 3(b) where subscript i represents ascending order of frequency, $f_{n,fw}$ and $f_{n,bw}$ nutational frequencies of the vortices with forward and backward rolling, respectively, f_p precessional frequency of vortices, $f_{d,l}$ frequency of the long wave in droplet motion, $f_{d,s}$ frequency of the short wave (wiggle) in droplet motion, $f_{d,am}$ frequency of amplitude modulation of the short wave in droplet motion.

$f_{\mathrm{low},1}$ (Hz)	$f_{\mathrm{low},2}$ (Hz)	$f_{\mathrm{high},1}$ (Hz)	$f_{high,2}$ (Hz)	$f_{high,3}$ (Hz)	$(f_{high,1}+f_{\mathrm{high},3})/2$ (Hz)	$(f_{high,1}-f_{high,3})/2$ (Hz)	$f_{n,\mathrm{fw}}$ (Hz)	$f_{n,\mathrm{bw}}$
0.351	0.703	4.57	5.16	5.51	5.04	0.47	4.51 ± 0.19	6.01 ± 0.85
f_p (Hz)	$f_{d,l}$ (Hz)		$f_{d,am}$ (Hz)	$f_{d,s}$ (Hz)	$(f_{n,bw}+f_{n,fw})/2$ (Hz)	$(f_{n,bw}-f_{n,fw})/2$ (Hz)		
0.326	0.333		0.335	5.46 ± 0.43	5.26 ± 0.52	0.75 ± 0.50		

First, we must consider the transition state from the first stage of droplet motion to the second stage, shown in Fig. 2(b). The vortex pair rotates along the droplet surface with oscillation at slightly different oscillation frequencies, as shown in Fig. 5. Furthermore, as discussed above, the vortex pair has a mass; therefore, we can consider the oscillating vortex pair as coupled oscillators. Oscillation characteristics of the vortex pair and the droplet in the transition state are summarized in Table II. in which $f_{\mathrm{low},i}$ and $f_{\mathrm{high},i}$ are lower and higher frequencies of droplet motion at the peaks of the frequency spectrum in Fig. 3(b), where subscript i represents the ascending order of frequency, and $f_{n,fw}$ and $f_{n,bw}$ are nutational frequencies of the vortices with forward and backward rolling, respectively, f_p is precessional frequency of the vortices, $f_{d,l}$ is the frequency of the long wave in droplet motion, $f_{d,s}$ is the frequency of the short waves (wiggle) in droplet motion, and $f_{d,am}$ is the frequency of amplitude modulation of the short waves in droplet motion. The correlation between the frequencies is summarized as follows:

(a) $f_{\mathrm{low},1}$ is almost the same as f_p, $f_{d,l}$, and $f_{d,am}$.

(b) $f_{\mathrm{high},1}$ and $f_{\mathrm{high},3}$ are almost identical to $f_{n,fw}$ and $f_{n,bw}$, respectively.

(c) The arithmetic mean of $f_{\mathrm{high},1}$ and $f_{\mathrm{high},3}$ has a similar value to $f_{\mathrm{high},2}$.

(d) The arithmetic mean (c) is almost equal to $f_{d,s}$.

(e) The half value of the difference between $f_{\mathrm{high},1}$ and $f_{\mathrm{high},3}$ or $f_{n,fw}$ and $f_{n,bw}$ is similar to $f_{\mathrm{low},1}$.

In general, coupled oscillators with slightly different eigenfrequencies exhibit a beat phenomenon. The oscillators oscillate at the frequency of the arithmetic mean of each frequency, and the beat period is equal to the half value of the difference between each frequency [40]. Correlation (a) indicates that the low frequency in the spectrum of droplet motion represents the slow rotation (the long wave) of the droplet, and the precession of the vortex pair induces motion. According to correlation (b), high frequencies in the spectrum of droplet motion correspond to nutation of the vortex pair. According to correlations (c) and (d), vortex nutation gives rise to the wiggle (short wave) of the droplet. Furthermore, according to the correlation (e), interaction of the vortex pair with nutation induces the beat phenomenon of droplet motion. To sum up the correlation, we found that the vortex pair made the droplet rotate with the precessional frequency of the vortex, and oscillate with the frequency of the arithmetic mean of the nutation frequencies. The vortex pair, which has different nutational frequencies, acts as coupled oscillators, and the interaction between the vortex pair induces amplitude modulation of the short waves. When the frequency of the amplitude modulation of nutation becomes equal to the precessional frequency of the vortex pair, resonant interaction occurs between the long wave and the envelope of the short waves. As a result, the third stage of droplet motion starts, and regular and fast rotation of the droplet occurs, as shown in Fig. 2[(B)c].

For volumetric flow rates, 25 and 100 μL/min, the frequency spectrum in the transition state follows a similar evolution for the volumetric flow rate of 50 μL/min (data not shown). The result indicates that the regular and fast rotation of a droplet occurs when vortex motion satisfies resonant conditions. Furthermore, such dissipative structures are not specific to the present systems, and can occur in remarkably different systems in which reactions occur at the droplet surface [25]. The tendency for dynamical interfacial tension to increase with time is common to these systems [28]. If any systems satisfy the conditions for the onset of eruption and to maintain the steady velocity profile of internal flow, the droplets can continue to move.

V. CONCLUSION

We have presented experimental results on the interfacial instability of a pendant droplet during mass transfer with solution supply. Self-organized flow inside the droplet occurs as the droplet grows bigger, and develops to a vortex pair. These vortices, exhibiting motionlike precession accompanied by nutation of a spinning top about a fixed point, interact with each other and behave as coupled oscillators. Precession induces slow rotation (long wave) of the droplet, and nutation induces wiggle (short wave). While the vortex pair rotates, the nutational amplitude of the vortex pair changes. Eventually, when the precessional period becomes equal to the period of the amplitude modulation of nutation, resonant interaction occurs between the long wave and the envelope of the short waves. As a result, the droplet rotates rapidly.

The instability phenomena in the present study develop hydrodynamically; hence, similar instability can occur in large-scale dynamics. If a pair of typhoons large enough to revolve around a star exists in the star, the star may deviate far from its stable orbit.

ACKNOWLEDGMENTS

We thank Professor Akihisa Shioi of the Department of Chemical Engineering & Materials Science of Doshisha University for fruitful discussions and Mr. Tadashi Mitani for analyzing droplet motion. T.B. is grateful for support from the Japan Society for the Promotion of Science (JSPS).

[1] L. Rayleigh, Philos. Mag. **32**, 529 (1916).
[2] J. R. A. Pearson, J. Fluid Mech. **4**, 489 (1958).
[3] C. V. Sternling and L. E. Scriven, AIChE J. **5**, 514 (1959).
[4] L. E. Scriven and C. V. Sternling, J. Fluid Mech. **19**, 321 (1964).
[5] G. E. Goltz, J. Imp. Coll. Chem. Eng. Soc. **12**, 40 (1958).
[6] H. Sawistowski, *Recent Advances in Liquid-Liquid Extraction*, edited by C. Hanson (Pergamon Press, Oxford, 1971), Chap. 9.
[7] J. B. Lewis and H. R. C. Pratt, Nature (London) **171**, 1155 (1953).
[8] H. Heines and J. W. Westwater, Int. J. Heat Mass Transfer **15**, 2109 (1972).
[9] J. B. Lewis, Chem. Eng. Sci. **3**, 248 (1954).
[10] N. G. Maroudas and H. Sawistowski, Chem. Eng. Sci. **19**, 919 (1964).
[11] C. A. P. Bakker, F. H. Fentener van Vlissingen, and W. J. Beek, Chem. Eng. Sci. **22**, 1349 (1967).
[12] I. Komasawa, T. Saito, and T. Otake, Kagaku (Kyoto, Jpn.) **35**, 1125 (1971).
[13] D. R. Olander and L. B. Reddy, Chem. Eng. Sci. **19**, 67 (1964).
[14] D. A. Haydon, Proc. R. Soc. London, Ser. A **243**, 483 (1958).
[15] T. V. Davies and D. A. Haydon, Proc. R. Soc. London, Ser. A **243**, 492 (1958).
[16] T. S. Sorensen, M. Hennenberg, A. Steinchen, and A. Sanfeld, J. Colloid Interface Sci. **56**, 191 (1976).
[17] T. Ondarcuhu and M. Veyssie, J. Phys. II **1**, 75 (1991).
[18] M. K. Chaudhury and G. M. Whitesides, Science **256**, 1539 (1992).
[19] K. Yoshikawa and N. Magome, Bull. Chem. Soc. Jpn. **66**, 3352 (1993).
[20] F. Domingues Dos Santos and T. Ondarcuhu, Phys. Rev. Lett. **75**, 2972 (1995).
[21] S. W. Lee and P. E. Laibinis, J. Am. Chem. Soc. **122**, 5395 (2000).
[22] Y. Sumino, N. Magome, T. Hamada, and K. Yoshikawa, Phys. Rev. Lett. **94**, 068301 (2005).
[23] T. Ban, F. Kawaizumi, S. Nii, and K. Takahashi, Chem. Eng. Sci. **55**, 5385 (2000).
[24] A. Shioi, K. Yamada, R. Shiota, F. Hase, and T. Ban, Bull. Chem. Soc. Jpn. **79**, 1696 (2006).
[25] T. Ban, T. Fujii, K. Kurisaka, and A. Shioi, Chem. Lett. **35**, 1134 (2006).
[26] T. Ban, S. Suzuki, S. Abe, and A. Shioi, Chem. Lett. **36**, 1040 (2007).
[27] T. Ban, T. Kita, H. Tominaga, and A. Shioi, Chem. Lett. **36**, 1134 (2007).
[28] T. Ban and A. Shioi, *Chemical Reactions on Surfaces*, edited by F. Columbus (NOVA Science Publishers, New York, 2008).
[29] T. Toyota, H. Tsuha, K. Yamada, K. Takakura, K. T. Ikegami, and T. Sugawara, Chem. Lett. **35**, 708 (2006).
[30] M. M. Hanczyc, T. Toyota, T. Ikegami, N. Packard, and T. Sugawara, J. Am. Chem. Soc. **129**, 9386 (2007).
[31] V. G. Levich, *Physicochemical Hydrodynamics* (Prentice-Hall, Englewood Cliffs, NJ, 1962).
[32] Song-I. Han, S. Stapf, and B. Blumich, Phys. Rev. Lett. **87**, 144501 (2001).
[33] See EPAPS Document No. E-PLEEE8-79-113902 for movies showing vortex dynamics and mass transfer behavior. For more information on EPAPS, see http://www.aip.org/pubservs/epaps.html.
[34] W. J. Korchinsky and C. H. Young, Chem. Eng. Sci. **41**, 3053 (1986).
[35] C. Chien-Hsiang and I. F. Elias, Colloids Surf., A **100**, 1 (1995).
[36] J. Hosokawa, H. Azuma, E. Iwata, T. Ban, and A. Shioi, J. Chem. Eng. Jpn. **39**, 1115 (2006).
[37] J. M. Burgers, Adv. Appl. Mech. **1**, 171 (1948).
[38] T. Tatsumi, *Ryutairikigaku* (Baifukan, Tokyo, 1982).
[39] I. Imai, *Ryutairikigaku* (Shokabo, Tokyo, 1973).
[40] K. Kondo, *Shindoron* (Baihukan, Tokyo, 1993).